

01 Mar 2014

## Receiver Function Constraints on Crustal Seismic Velocities and Partial Melting beneath the Red Sea Rift and Adjacent Regions, Afar Depression

Cory A. Reed

Sattam Almadani

Stephen S. Gao

Missouri University of Science and Technology, [sgao@mst.edu](mailto:sgao@mst.edu)

Ahmed A. Elsheikh

*et. al.* For a complete list of authors, see [https://scholarsmine.mst.edu/geosci\\_geo\\_peteng\\_facwork/407](https://scholarsmine.mst.edu/geosci_geo_peteng_facwork/407)

Follow this and additional works at: [https://scholarsmine.mst.edu/geosci\\_geo\\_peteng\\_facwork](https://scholarsmine.mst.edu/geosci_geo_peteng_facwork)



Part of the [Geology Commons](#), and the [Numerical Analysis and Scientific Computing Commons](#)

### Recommended Citation

C. A. Reed et al., "Receiver Function Constraints on Crustal Seismic Velocities and Partial Melting beneath the Red Sea Rift and Adjacent Regions, Afar Depression," *Journal of Geophysical Research: Solid Earth*, vol. 119, no. 3, pp. 2138-2152, John Wiley & Sons Ltd, Mar 2014.

The definitive version is available at <https://doi.org/10.1002/2013JB010719>

This Article - Journal is brought to you for free and open access by Scholars' Mine. It has been accepted for inclusion in Geosciences and Geological and Petroleum Engineering Faculty Research & Creative Works by an authorized administrator of Scholars' Mine. This work is protected by U. S. Copyright Law. Unauthorized use including reproduction for redistribution requires the permission of the copyright holder. For more information, please contact [scholarsmine@mst.edu](mailto:scholarsmine@mst.edu).

## RESEARCH ARTICLE

10.1002/2013JB010719

## Key Points:

- Strain in the lower crust is diffuse, while upper crustal strain is localized
- The Red Sea rift axis likely migrated eastward gradually since the late Miocene
- The lower crust beneath the Red Sea rift is decoupled from the upper crust

## Correspondence to:

C. A. Reed,  
caryrd@mst.edu

## Citation:

Reed, C. A., S. Almadani, S. S. Gao, A. A. Elsheikh, S. Cherie, M. G. Abdelsalam, A. K. Thurmond, and K. H. Liu (2014), Receiver function constraints on crustal seismic velocities and partial melting beneath the Red Sea rift and adjacent regions, Afar Depression, *J. Geophys. Res. Solid Earth*, 119, 2138–2152, doi:10.1002/2013JB010719.

Received 24 SEP 2013

Accepted 24 FEB 2014

Accepted article online 27 FEB 2014

Published online 25 MAR 2014

## Receiver function constraints on crustal seismic velocities and partial melting beneath the Red Sea rift and adjacent regions, Afar Depression

Cory A. Reed<sup>1</sup>, Sattam Almadani<sup>1,2</sup>, Stephen S. Gao<sup>1</sup>, Ahmed A. Elsheikh<sup>1</sup>, Solomon Cherie<sup>3,1</sup>, Mohamed G. Abdelsalam<sup>1,4</sup>, Allison K. Thurmond<sup>5</sup>, and Kelly H. Liu<sup>1</sup>

<sup>1</sup>Geology and Geophysics Program, Missouri University of Science and Technology, Rolla, Missouri, USA, <sup>2</sup>Now at Geology and Geophysics Department, College of Science, King Saud University, Riyadh, Saudi Arabia, <sup>3</sup>Geological Survey of Ethiopia, Addis Ababa, Ethiopia, <sup>4</sup>Now at Boone Pickens School of Geology, Oklahoma State University, Stillwater, Oklahoma, USA, <sup>5</sup>Global Basin Analysis, Statoil, ASA, Bergen, Norway

**Abstract** The Afar Depression is an ideal locale for the investigation of crustal processes involved in the transition from continental rifting to oceanic spreading. To provide relatively high resolution images of the crust beneath the Red Sea rift (RSR) represented by the Tendaho graben in the Afar Depression, we deployed an array of 18 broadband seismic stations in 2010 and 2011. Stacking of about 2300 receiver functions from the 18 and several nearby stations along the ~200 km long array reveals an average crustal thickness of  $22 \pm 4$  km, ranging from ~17 km near the RSR axis to 30 km within the overlap zone between the Red Sea and Gulf of Aden rifts. The resulting anomalously high  $V_p/V_s$  ratios decrease from 2.40 in the southwest to 1.85 within the overlap zone. We utilize theoretical  $V_p$  and melt fraction relationships to obtain an overall highly reduced average crustal  $V_p$  of ~5.1 km/s. The melt percentage is about 10% beneath the RSR while the overlap zone contains minor quantities of partial melt. The observed high  $V_p/V_s$  values beneath most of the study area indicate widespread partial melting beneath the southwest half of the profile, probably as a result of gradual eastward migration of the RSR axis. Our results also suggest that the current extensional strain in the lower crust beneath the region is diffuse, while the strain field in the upper crust is localized along narrow volcanic segments. These disparate styles of deformation imply a high degree of decoupling between the upper and lower crust.

## 1. Introduction

### 1.1. Tectonic Setting

The Afar Depression of northeastern Africa possesses a classic example of a subaerial rift-rift-rift triple junction [McKenzie *et al.*, 1970] forming as the result of the intersection of the Red Sea and Gulf of Aden rift arms and the Main Ethiopian rift (MER). Locally, however, only the Red Sea and Main Ethiopian rifts interact directly (Figure 1a) since the Gulf of Aden rift arm propagates landward farther to the north [Courtilot *et al.*, 1987; Manighetti *et al.*, 1997; Manighetti *et al.*, 1998]. This rift system forms the current tectonic boundary between the Nubian Plate to the west, the Somalian Plate to the southeast, and the Arabian Plate toward the northeast [Chase, 1978; Stein and Gordon, 1984].

Onset of voluminous Oligocene flood basalts and rhyolitic ignimbrite sequences at about 30 Ma [Baker *et al.*, 1996; Hofmann *et al.*, 1997; Ayalew *et al.*, 2002] was approximately coeval with extension in the Gulf of Aden [Ebinger and Sleep, 1998; Bosworth *et al.*, 2005] and was synchronous with or immediately preceded the beginning of extension in the southernmost Red Sea rift (RSR) between 29 Ma and 26 Ma [Wolfenden *et al.*, 2005]. Recent volcanism is limited primarily to segments within the Red Sea and Gulf of Aden rifts, which have advanced landward through a series of discrete jumps [Lahitte *et al.*, 2003], though significant off-axis magmatic low-velocity zones have been reported [Stork *et al.*, 2013]. Initiation of extension in the northern MER did not originate until 11–10 Ma, during which time the MER linked with southern Afar marginal fault belts, producing a paleo-triple junction at ~10°N [Tesfaye *et al.*, 2003]. Since that time, northeastward migration of the Afar triple junction has resulted in a present-day location at approximately 11.5°N at the contact of the northern MER and the Tendaho-Gobaad Discontinuity (Figure 1a) [Tesfaye *et al.*, 2003; Wolfenden *et al.*, 2004].

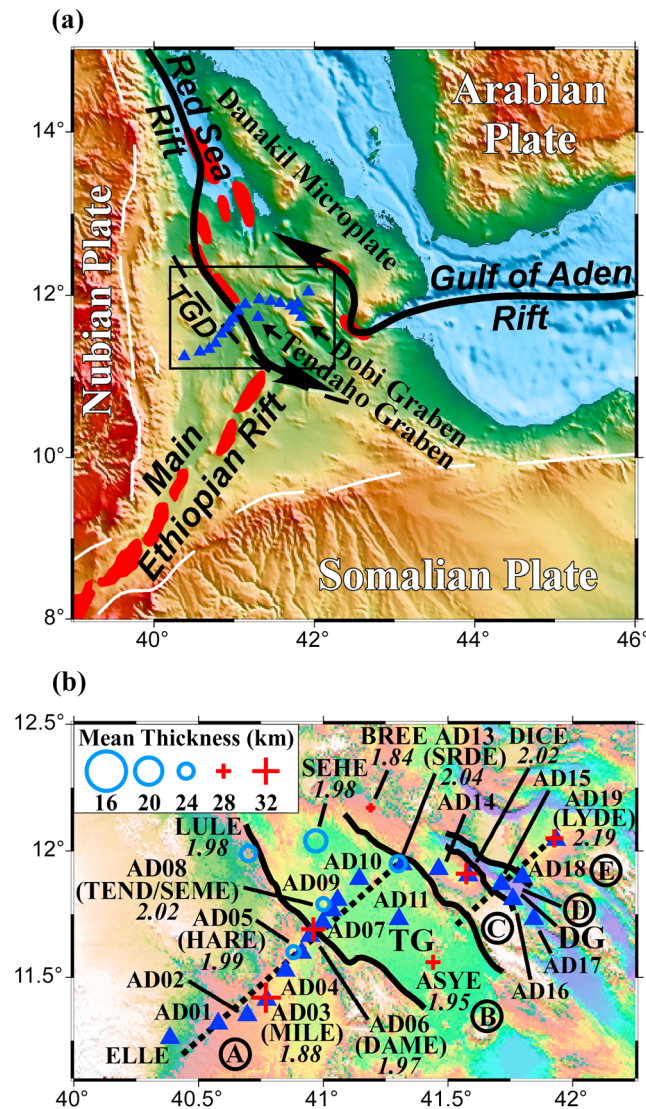


**Figure 1.** (a) Topographic map of the Afar Depression showing major tectonic features and locations of seismic stations. Solid white lines indicate Miocene border faults, solid black lines denote axes of the Red Sea and Gulf of Aden rifts, red polygons indicate subaerial magmatic provinces, and blue triangles represent seismic stations. TGD = Tendaho Gobaad Discontinuity separating east-central Afar from southwestern Afar. (b) Topographic map of the study area (rectangle in Figure 1a) with names of the ALIE stations and the bisected cross-section profile (dashed black lines). Colocated stations are listed in parentheses, and regions are denoted by their respective letters circumscribed within circles. Open circles and crosses represent previous crustal thickness observations, and italicized numbers indicate  $V_p/V_s$  measurements from Hammond et al. [2011]. TG = Tendaho graben, DG = Dobi graben.

The RSR extends to the southeast in the Afar Depression as the Manda Hararo-Gobaad rift system [Varet, 1978; Thurmond et al., 2006], represented at its southeasternmost extent by the Tendaho graben. The Afar Stratoid series, comprised of basaltic extrusives with minor rhyolitic contributions spanning 4 to 1 Ma [Varet, 1978], initiated eruption within the Tendaho graben at approximately 2 Ma during a period of rift-synchronous volcanism [Abbate et al., 1995; Acton et al., 2000; Acocella et al., 2008]. The graben is bounded by flanks of extruded Stratoid basalts, while the interior basin is infilled with at least 1.6 km of lacustrine sediment as well as Pleistocene post-Stratoid basaltic flows [Varet, 1978; Abbate et al., 1995]. Farther to the northeast, the Dobi graben comprises the northwesternmost extent of the NW-SE trending Dobi-Hanle rift system, which bears structural similarity to the Tendaho graben and is thought to have formed through similar mechanisms [Abbate et al., 1995; Acocella, 2010]. Farther beyond the Dobi-Hanle rift system to the northeast lies a zone of broad, diffusely extended continental crust overlain with the Stratoid series bounded to the southwest and northeast by the Dobi-Hanle and Gulf of Aden rifts, respectively. This ~100 km wide overlap zone has been previously interpreted as multiple rigid, clockwise-rotating microplates produced as a result of strain distribution between the competing rift propagators through regional-scale bookshelf faulting [Tapponnier et al., 1990; Acton et al., 1991; Sigmundsson, 1992; Manighetti et al., 2001]. Further details about the tectonic framework and evolution of the study area can be found in Beyene and Abdelsalam [2005] and Bosworth et al. [2005].

A multitude of studies have been conducted to reveal the distribution of strain throughout the Afar Depression and the MER. It has been widely accepted that approximately 80–85% of strain within the Afar is restricted to disconnected rift segments [Manighetti et al., 2001]. Similar results have been obtained for the MER, where it has also been proposed that the locus of extensional strain in the upper crust has been concentrated greatly (greater than 80% of the total strain field) on magmatic segments [Ebinger and Casey, 2001] associated with a Quaternary zone of faulting approximately 33 km wide [Bilham et al., 1999] collectively known as the Wonji Fault Belt [Pizzi et al., 2006], thus leading to modern-day strain abandonment along the MER border faults. Significant evidence to support these hypotheses has been provided by imagery of rift-axial elongate dike emplacements and subvolcanic magma chambers using

gravity [Cornwell *et al.*, 2006] and controlled source seismic profiles [Makris and Ginzburg, 1987; Keranen *et al.*, 2004; Mackenzie *et al.*, 2005] in both the Afar and the MER.

However, considerable evidence has been observed to the contrary of axially localized extension. Seismicity within the MER constrained by  $b$  values [Keir *et al.*, 2006a] and by accurate earthquake foci determinations [Keir *et al.*, 2009a] demonstrates the facilitation of seismicity by partial melt within the lower crust as well as the occurrence of notable seismic activity along rift border faults. These observations, when integrated with Quaternary magmatism and partial melt throughout the crust along the northwestern MER border fault system [Rooney *et al.*, 2007] as well as off-axis conductive bodies beneath the Northern Plateau [Whaler and Hautot, 2006], indicate that a significant measure of strain is not concentrated within the MER axis but is somewhat widespread. Additionally, geodetic observations and modeling from Kogan *et al.* [2012] indicate that extension in the Afar is occurring over a zone approximately 175 km wide coincident with an absence of the mantle lithosphere. The same study discovered a strain field of  $\sim 85$  km width across the northern MER, extending well beyond the rift border faults, which is underlain by anomalously thinned lithosphere [Dugda *et al.*, 2007]. Furthermore, a study conducted by Keir *et al.* [2011] on an off-axis rift-orthogonal magmatic injection indicates that the current distribution of strain within the northern and central Afar is not wholly localized within the present-day locus of extensional strain.

### 1.2. Previous Geophysical Investigations of Afar Crust

Using data from a seismic refraction profile directed alongstrike to the Tendaho graben, Makris and Ginzburg [1987] observed an  $\sim 3$  km thick sedimentary cover with  $P$  wave velocities of 3.35 km/s and a basalt layer with a  $V_p$  of 4.5 km/s extending to a depth of  $\sim 6$  km toward the RSR axis with a thinned upper crust of approximately 4 km thickness. The refraction profile, however, did not traverse the entire graben and hence did not obtain a viable variation of crustal structure across the rift axis. Refraction results from a profile, sourced near Assab in southeastern Eritrea with a WSW strike directed toward the Tendaho graben, inferred a crustal thickness between 26 and 28 km beneath the overlap zone but did not extend fully to the RSR.

Only a few receiver function (RF) analyses have been conducted within the study area to examine variations in crustal thickness ( $H$ ) and the  $P$  to  $S$  wave velocity ratio ( $V_p/V_s$ , hereafter denoted  $\kappa$ ) [Dugda *et al.*, 2005; Hammond *et al.*, 2011]. The seismic stations used in these studies were well over tens of kilometers apart (Figure 1b), which prevented an analysis possessing good resolution of the RSR crust. Furthermore, different average crustal  $V_p$  values were utilized in the stacking of the RFs, leading to an inconsistency in the resulting  $H$  and  $\kappa$  measurements. For the study area, the  $V_p$  values used by Hammond *et al.* [2011] ranged between 6.15 km/s and 6.25 km/s, while Dugda *et al.* [2005] employed a constant  $V_p$  of 6.50 km/s. The  $\kappa$  values obtained by previous studies in our region rise as high as 2.31, which is significantly larger than those found beneath most continental areas and suggests the existence of vast quantities of partial melt within the crust [Hammond *et al.*, 2011]. As discussed in the next section, some of the higher average crustal  $V_p$  values used in previous studies within the east-central Afar may not be compatible with theoretically determined  $P$  velocities for crustal lithologies containing partial melt.

A number of hypotheses concerning the nature of the crust underlying the Afar Depression have been proposed. Makris and Ginzburg [1987] proposed a model for the Afar consisting of seismic velocities characteristic of extraordinarily thinned continental crust intruded with extensive mafic diking. Receiver function constraints from Hammond *et al.* [2011] imply isolated blocks of continental composition between the Red Sea and Gulf of Aden propagators, along which oceanic-type crust is currently being generated. Numerous models regarding the generation of oceanic lithosphere with the onset of incipient seafloor spreading within the rift axial zones have been advocated [McKenzie *et al.*, 1970; Barberi and Varet, 1977; Prodehl *et al.*, 1997; Stuart *et al.*, 2006; Bastow *et al.*, 2011]. Others have argued that the Afar Depression is marked by unique transitional continental spreading leading to the formation of new magmatic crust [Mohr, 1989; Kazmin and Byakov, 2000], which possibly originated around 16 Ma [Wolfenden *et al.*, 2005] and has been shown to generate oceanic-type magnetic anomaly patterns [Bridges *et al.*, 2012].

### 1.3. Crustal Seismic Velocities and Melt

Fluid fractions within a medium have been shown to be clearly identifiable through the application of the velocity ratio  $\kappa$ , specifically with regard to a silicate melt [Watanabe, 1993]. The  $\kappa$  value is a continuous function of the melt fraction, with a normal increase in the fluid percentage resulting in an exponential increase in  $\kappa$  as a consequence of the rapid reduction of  $V_s$  relative to  $V_p$  (Figure 2). According to the Watanabe [1993] study, for dry bulk crustal conditions, an average  $V_p$  of 6.15 km/s corresponds to a  $\kappa$  of 1.82, wherein the

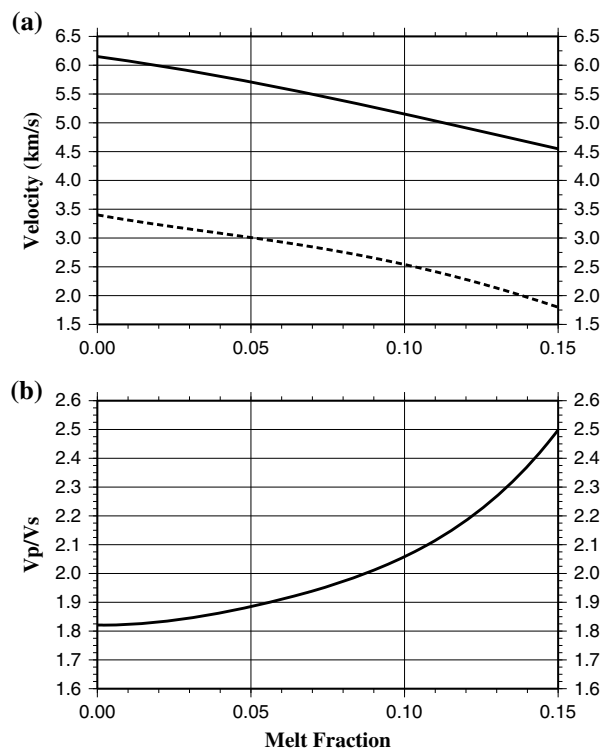


**Figure 2.** Theoretical curves showing variations of (a)  $P$  wave (solid line) and  $S$  wave (dashed line) velocities and (b)  $V_p/V_s$  ( $\kappa$ ) as a function of volume melt fraction (modified from *Watanabe* [1993]).

fractions corresponding to higher  $\kappa$  values. This would not result in a significant alteration of the relative melt fraction distribution, and thus, our results would only differ in the inferred melt quantity present beneath the RSR.

The theoretical velocity-melt relationship developed by *Watanabe* [1993] has been successfully applied to constrain melt restricted to the crust in numerous tectonic regions, including the Altiplano [*Yuan et al.*, 2002], Japan [*Nakajima et al.*, 2001], and Tibet [*Makovsky and Klempnerer*, 1999; *Li et al.*, 2003; *Caldwell et al.*, 2009]. In addition, the pre-melt  $V_p$  and  $\kappa$  values used in *Watanabe* [1993] are comparable with typical  $V_p$  values used for RF stacking and the resulting  $\kappa$  values beneath continental areas such as the Limpopo belt in southern Africa [*Nair et al.*, 2006] and the Colorado Plateau and the Basin and Range Province in North America [*Bashir et al.*, 2011].

This study analyzes data from a relatively dense broadband seismic array across the Tendaho graben in order to provide crustal thickness and  $\kappa$  measurements using station-specific mean crustal  $V_p$ . Using these observations, we then estimate the volume and the distribution of melting to investigate the nature of the crust underlying the RSR as well as qualify the localization of strain and the existence of upper-lower crustal coupling beneath the study area. By comparing the RSR to typical mid-ocean ridges and continental rifts, our results provide additional constraints on the hypothesis that the RSR is in a transitional stage to an oceanic spreading center. It is necessary, however, to specify that our profile traverses a complex area affected by the interaction of three rift propagators, and thus, our results and conclusions may not be readily applicable to typical continental rifts or to other regions within the Afar or the MER.

## 2. Data and Methods

### 2.1. Data

Most of the three-component broadband seismograms used in the study were recorded at 18 stations belonging to the Afar Lithosphere Imaging Experiment (ALIE) project that we operated from early 2010 to May 2011. The stations were along an array approximately 200 km long possessing an average

melt fraction is zero. Values of  $\kappa$  greater than 1.82 must theoretically, without accounting for source composition, temperature, or melt geometry (see *Clemens and Vielzeuf* [1987], *Hammond and Humphreys* [2000], and *Takei* [2002] for further references), relate to increasing degrees of partial melt located within the crust and a correlative decrease in  $V_p$ . For instance, an 11% melt volume results in a  $\kappa$  of approximately 2.12 with an associated  $V_p$  of 5.0 km/s (Figure 2).

The *Watanabe* [1993] study assumes a granitic substrate intruded with varying quantities of rhyolitic melt. However, magma of bimodal composition has been observed within Ethiopia, notably mafic melt associated with flood basalts and shallower fractionated rhyolitic magma chambers [*George et al.*, 1998; *Ayalew et al.*, 2002; *Lahitte et al.*, 2003; *Rooney et al.*, 2012b]. Thus, a study focused on silicic melt may not be completely applicable to the Afar Depression. A change in melt composition, however, would result in an approximately linear translation of the  $\kappa$ -melt fraction curve (Figure 2b) and subsequently lower melt

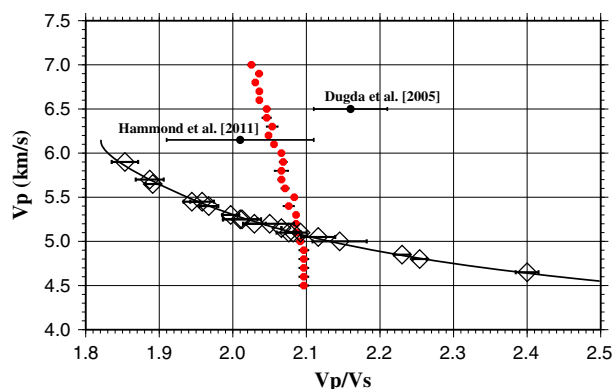


**Figure 3.** Theoretical (solid line, based on *Watanabe* [1993]) and observed (solid red dots with error bars, from global stacking)  $V_p$  as a function of  $\kappa$ . Open diamonds represent observed  $V_p$ - $\kappa$  pairs from this study, and solid black dots show those from previous studies. Results from *Dugda et al.* [2005] are from station TEND located in central Afar, while those of *Hammond et al.* [2011] are the averages of all stations located within our profile as well as of their stations BTIE, LULE, SEHE, BREE, and ASYE.

HARE, and DAME (colocated with AD03, AD05, and AD06, respectively) were combined with the ALIE data set. Four stations from the Afar Consortium Network also contributed data used in this study, two of which (SRDE and LYDE) are colocated with ALIE stations (AD13 and AD19, respectively), whereas ELLE and DICE are independently integrated within the profile (Figure 1b).

Data utilized for this study were archived by and requested from the Incorporated Research Institutions for Seismology (IRIS) Data Management Center (DMC). Data for all events with epicentral distances between  $30^\circ$  and  $180^\circ$  over the period from early-2000 to mid-2012 were requested from the DMC. A cutoff magnitude, which is defined as  $M_c = 5.2 + (D_e - 30.0)/(180.0 - 30.0) - H_f/700$ , where  $D_e$  and  $H_f$

station spacing of about 12 km (Figure 1b). Each station was equipped with a 120 s Guralp CMG-3T three-component broadband sensor which recorded continuously with a sampling frequency of 100 Hz. The data set was expanded with the addition of data from station TEND from the Ethiopia-Kenya Broadband Experiment (2000–2002) [*Nyblade and Langston*, 2002] and station SEME from the Boina Broadband Network (2005–2006) and AFAR07 (2007–2009) [*Ebinger et al.*, 2010] experiments. The two non-ALIE stations (TEND and SEME) were located approximately 3 km from AD08, and as a result the data from the three stations are merged for joint analyses. Similarly, data from other AFAR07 stations MILE,

are the event epicentral distance and focal depth, respectively, was applied to the request. A minimum  $M_c$  of 4.2 corresponds with a  $D_e$  and  $H_f$  of  $30^\circ$  and 700 km, respectively, while a maximum  $M_c$  of 6.2 is obtained for corresponding values of  $180^\circ$  and 0 km depth. This cutoff magnitude dependency upon event epicentral distance and focal depth is applied for the purpose of taking advantage of higher-quality waveforms sourced from deeper earthquakes [*Liu and Gao*, 2010].

Seismograms were windowed to 20 s prior to and 340 s following the predicted arrival of the first compressional wave phase based upon the IASP91 Earth model. A 4 pole, 2 pass band-pass filter with corner frequencies of 0.04 and 1.0 Hz was applied to the three-component seismograms during a preliminary phase search and subsequent RF calculations to improve the signal-to-noise ratio (SNR), and seismograms with an

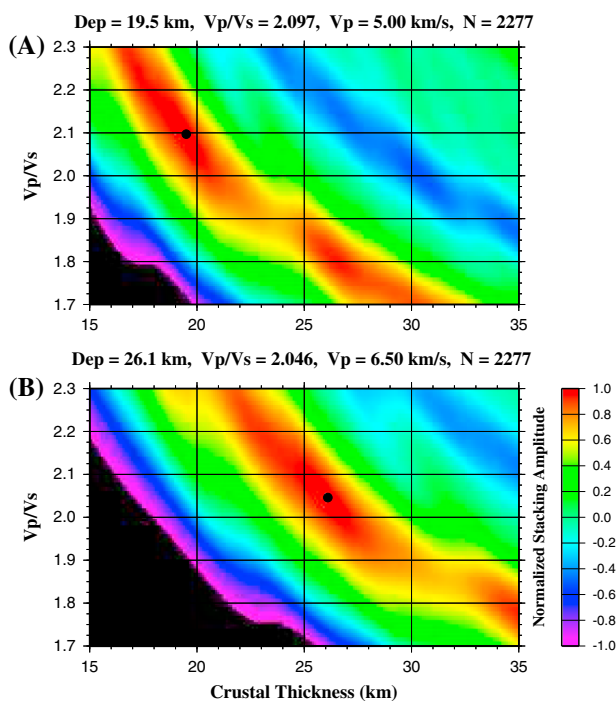


**Figure 4.**  $H$ - $\kappa$  stacks using all of the 2277 RFs. Black dots indicate locations of maximum stacking amplitudes. (a)  $V_p = 5.0$  km/s. (b)  $V_p = 6.5$  km/s.

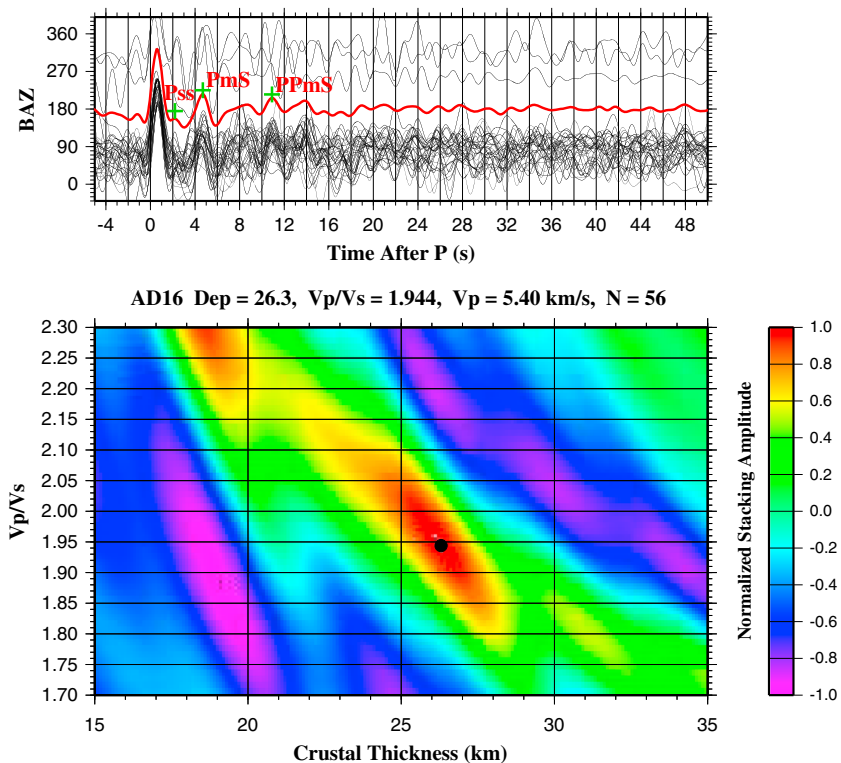


**Figure 5.** (Top) Individual receiver functions (black) plotted against back azimuth for station AD16, located in the Dobi graben. The red trace represents a simple time domain stack of all RFs recorded at the station. Green crosses indicate the arrival time of the respective phases. Note the arrival associated with the  $P_{ss}$  phase, indicating weak sedimentary reverberations. (Bottom)  $H$ - $\kappa$  plot.

SNR less than 4.0 were rejected. The remaining seismograms were converted into radial RFs utilizing the procedure of Ammon [1991]. Subsequently, visual checking removed RFs with questionable quality.

Multiple accounts of thick sedimentary layers exist for the study area, specifically with regard to Tendaho graben lacustrine infill exceeding 1.6 km thickness and sedimentary cover reaching up to 200 m on the Awsa plain east of the Red Sea Rift axis [Varet, 1978; Abbate et al., 1995]. Numerous receiver function studies have documented the existence of a  $P$  to  $S$  converted phase from the bottom of the sedimentary layer [Diehl et al., 2005; Mandal, 2006] which we denote  $P_{ss}$ . Due to the low  $P$  and especially  $S$  wave velocities, the layer has the ability to erroneously characterize the crustal thickness by a value approximately equivalent to the layer thickness [Yeck et al., 2013]. It is thus necessary to examine the RFs from each of the stations to determine whether the sedimentary layers have a detrimental effect on the signal.

An increase in the  $\kappa$  value for low-velocity sedimentary layers has been shown to lead to an increase in the time delay of the  $P_{direct}$  phase [Sheehan et al., 1995], while an increase in the thickness of the sedimentary layer will enhance the reverberatory (i.e., ringing) character of the signal following the  $P_{direct}$  arrival. Extremely high values of the Poisson's ratio ( $\sigma$ ), which is directly related to  $\kappa$  by the relationship  $\sigma = 0.5[1 - 1/(\kappa^2 - 1)]$  [Christensen, 1996], have been reported as large as 0.45 [Wang and Pan, 2001] and 0.49 [Kähler and Meissner, 1983] in unconsolidated sediment. These high  $\kappa$  values have the potential to mask the  $P_{ss}$  phase with high-amplitude, long-period multiples, rendering any attempt to utilize multiple-layer stacking futile. For a thorough review of the aforementioned phenomena and other effects of sedimentary layering on receiver functions, refer to Zelt and Ellis [1999].

In order to circumvent the effects of sediments on our  $H$ - $\kappa$  stacking, we subjected all converted radial receiver functions to two distinct filtering bands with corner frequencies of 0.08–0.8 Hz and 0.2–1.2 Hz with a 4 pole, 2 pass construct. As discussed below, 17 out of the 20 stations benefited from the latter

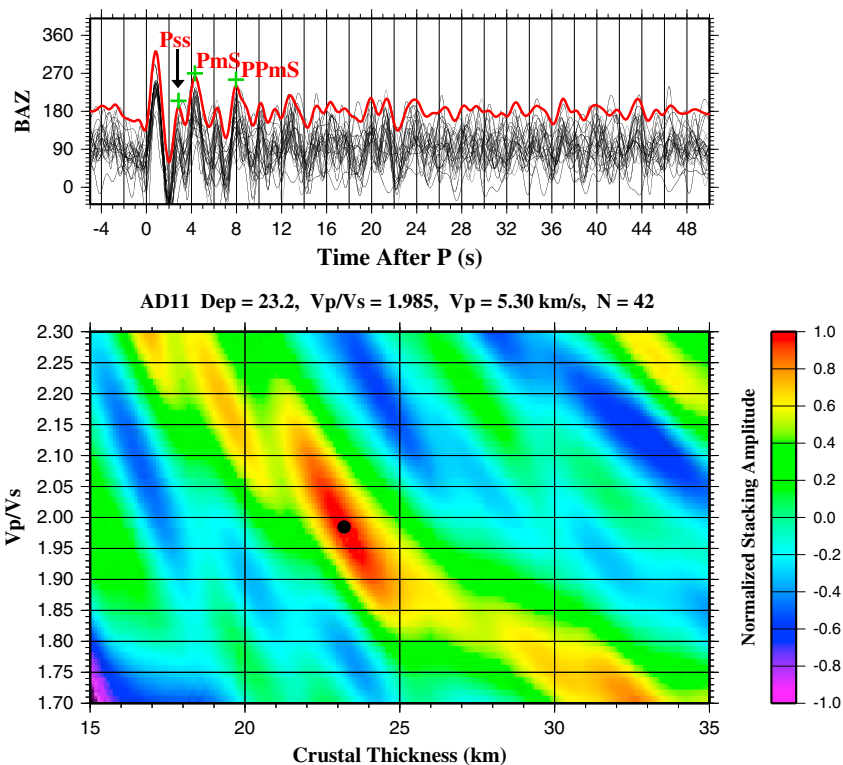


**Figure 6.** Same as the previous figure but for station AD11, located in the Tendaho graben. The receiver function stack demonstrates the arrival of a strong sedimentary  $P_{ss}$  reverberatory phase and high-amplitude ringing, as well as a higher  $P_{direct}$  time lag indicating a high sedimentary  $\kappa$ .

high-frequency band pass. Following the station-specific application of band-pass filters, we obtained a total of 2277 high-quality radial receiver functions for use in this study.

### 2.2. Stacking of Receiver Functions

The  $H$ - $\kappa$  stacking procedure applied here was developed based on the *Zhu and Kanamori [2000]* approach for RF moveout corrections and stacking. The procedure requires a mean crustal  $P$  wave velocity and computes moveout times for the  $P$ -to- $S$  converted phase ( $P_mS$ ) and its multiples ( $PP_mS$  and  $PS_mS$ ) at a series of combinations of candidate  $H$  (between 10 and 35 km with a step of 0.1 km) and  $\kappa$  (1.7 to 2.5 with a step of 0.01).

For each combination of  $H$  and  $\kappa$ , the RFs are stacked based upon weighted phase-specific moveout times, and the optimal combination of  $H$  and  $\kappa$  is the pair corresponding to the maximum stacking amplitude. Our recent applications of the procedure can be found in *Nair et al. [2006]*, *Liu and Gao [2010]*, and *Bashir et al. [2011]*. The weighting factors used for the stacking are 0.5, 0.4, and 0.1 for the  $P_mS$ ,  $PP_mS$ , and  $PS_mS$  phases, respectively. However, we find that for RFs recorded at station AD19, the  $P_mS$  phase has strong interference probably originating from surface or shallow heterogeneities, and consequently, we apply weighting factors of 0.2, 0.5, and 0.3 so that  $P_mS$  has a reduced contribution to the stacking.

We execute the stacking through 10 bootstrap resamplings as described by *Efron and Tibshirani [1986]* to obtain the optimal pair of  $H$  and  $\kappa$  and their standard errors. Each of the 10 bootstrap steps is conducted by first arbitrarily choosing approximately 63% of the receiver functions available from the station or group of stations considered. About 60% of these randomly chosen RFs are then duplicated and combined with the first randomized set, producing a quantity of available receiver functions which is equivalent to that of the original data set. Using the resulting  $H$ - $\kappa$  plots, the mean and standard deviation of both the crustal thickness and  $\kappa$  values are then calculated, which are expected to be normally distributed about the true  $H$  and  $\kappa$  values [*Press et al., 1992; Dugda et al., 2005; Nair et al., 2006; Liu and Gao, 2010*].



**Table 1.** Observations of Crustal Thickness ( $H$ ),  $V_p/V_s$  ( $\phi$ ),  $V_p$ , and Melt Fraction

Region	Station	Net	Lat. (deg)	Lon. (deg)	N	$H$ (km)	$\kappa$	$V_p$	Melt Fraction
A	ELLE	ZF	11.258	40.378	107	21.720 ± 0.110	2.092 ± 0.008	5.10	0.106
	AD01	ZK	11.315	40.571	64	18.530 ± 0.048	2.254 ± 0.010	4.80	0.128
	AD02	ZK	11.349	40.688	119	18.040 ± 0.097	2.082 ± 0.010	5.10	0.104
	AD03	ZK	11.422	40.766	190	18.150 ± 0.053	2.230 ± 0.011	4.85	0.126
	AD04	ZK	11.537	40.841	38	17.733 ± 0.082	2.400 ± 0.016	4.65	0.142
	AD05	ZK	11.608	40.906	287	20.600 ± 0.000	2.066 ± 0.000	5.15	0.102
	AD06	ZK	11.675	40.940	187	19.544 ± 0.194	2.050 ± 0.033	5.20	0.098
Average						19.278 ± 1.471	2.160 ± 0.126	5.04	0.114
B	AD07	ZK	11.727	40.990	42	20.750 ± 0.173	1.967 ± 0.013	5.40	0.078
	AD08	ZK	11.792	41.028	297	19.800 ± 0.221	2.076 ± 0.016	5.10	0.104
	AD09	ZK	11.817	41.050	100	17.620 ± 0.228	2.145 ± 0.037	5.00	0.115
	AD10	ZK	11.900	41.137	73	23.290 ± 0.120	1.891 ± 0.010	5.65	0.052
	AD11	ZK	11.741	41.296	42	23.100 ± 0.141	1.997 ± 0.011	5.30	0.086
	AD13	ZK	11.958	41.310	142	23.140 ± 0.361	1.958 ± 0.016	5.45	0.076
Average						21.283 ± 2.310	2.006 ± 0.091	5.32	0.085
C	AD14	ZK	11.939	41.455	47	23.190 ± 0.238	2.030 ± 0.016	5.20	0.094
	DICE	ZF	11.914	41.574	125	22.070 ± 0.392	2.116 ± 0.023	5.05	0.110
Average						22.630 ± 0.792	2.073 ± 0.061	5.12	0.102
D	AD15	ZK	11.880	41.707	20	22.520 ± 0.319	2.010 ± 0.024	5.25	0.090
	AD16	ZK	11.820	41.753	56	26.243 ± 0.181	1.944 ± 0.011	5.45	0.072
	AD17	ZK	11.742	41.837	106	24.250 ± 0.387	2.012 ± 0.026	5.25	0.090
Average						24.338 ± 1.863	1.989 ± 0.039	5.32	0.084
E	AD18	ZK	11.908	41.791	114	29.770 ± 0.189	1.887 ± 0.019	5.70	0.051
	AD19	ZK	12.054	41.926	121	30.456 ± 0.532	1.853 ± 0.018	5.90	0.034
Average						30.113 ± 0.485	1.870 ± 0.024	5.80	0.042
Global Average						22.264 ± 3.753	2.041 ± 0.131	5.28	0.090
Global Stack						19.950 ± 0.087	2.086 ± 0.007	5.07	0.105

### 3. Results

#### 3.1. Global Stacking

In order to obtain a first-order estimate of  $H$  and  $\kappa$  for the entire study area and to acquire an initial average crustal  $V_p$  for subsequent station-specific RF stacking, we perform global  $H$ - $\kappa$  stacking using all of the 2277 RFs by employing a series of  $V_p$  values ranging from 4.5 km/s to 7.0 km/s with a step of 0.1 km/s. The resulting  $\kappa$  versus  $V_p$  curve intersects with the theoretical curve at approximately  $\kappa = 2.09$  and  $V_p = 5.1$  km/s (Figure 3). Figure 4 shows results from two of the  $V_p$  steps. When a  $V_p$  value of 5.0 km/s is used (Figure 4a), an  $H$  of 19.5 km and  $\kappa$  of 2.097 are obtained; when  $V_p = 6.15$  km/s is used (Figure 4b), the corresponding values are 26.1 km and 2.046 km. Relative to the results from utilizing  $V_p = 5.0$  km/s, the  $H$  value increases by about 33.8% and the  $\kappa$  value decreases only by 2.5% when  $V_p = 6.15$  km/s is used. Note that the resulting  $H$  and  $\kappa$  values are heavily weighted by the area with the maximum number of RFs, which is the region southwest of the Tendaho graben having been sampled by several ALIE stations as well as stations from previous portable experiments.

An average crustal  $V_p$  of 5.1 km/s corresponds well with the approximate average  $V_p$  of three 6–10 km thick layers Ruegg [1975] discovered in the southeastern Afar. A  $V_p$  of 5.1 km/s is also in accordance with the observations of Makris and Ginzburg [1987] in which a thick low-velocity sedimentary cover reduces average crustal velocities within the rift zone.

#### 3.2. Individual Station Stacking

We next perform  $H$ - $\kappa$  stacking of RFs recorded by each of the stations for the purpose of characterizing spatial variations of crustal properties beneath the study area. To more accurately determine crustal thickness and  $\kappa$ , we use a two-step procedure. In the first step, a  $V_p$  of 5.1 km/s is used to obtain the initial  $H$  and  $\kappa$ . The latter is then used to constrain a more accurate  $V_p$  using the theoretical  $V_p$  versus  $\kappa$  relationship shown in Figure 3 (solid line). This revised  $V_p$  is then used in the second round of stacking to obtain the final  $H$  and  $\kappa$ . Note that this procedure takes advantage of the property of  $H$ - $\kappa$  stacking, as discussed previously, wherein  $\kappa$  is not sensitive to the chosen value of  $V_p$ . As expected, the  $V_p$  used for the second step and the resulting  $\kappa$  (Figure 3) follow the theoretical curve well, whereas the results of previous studies deviate significantly from the theoretical curve.

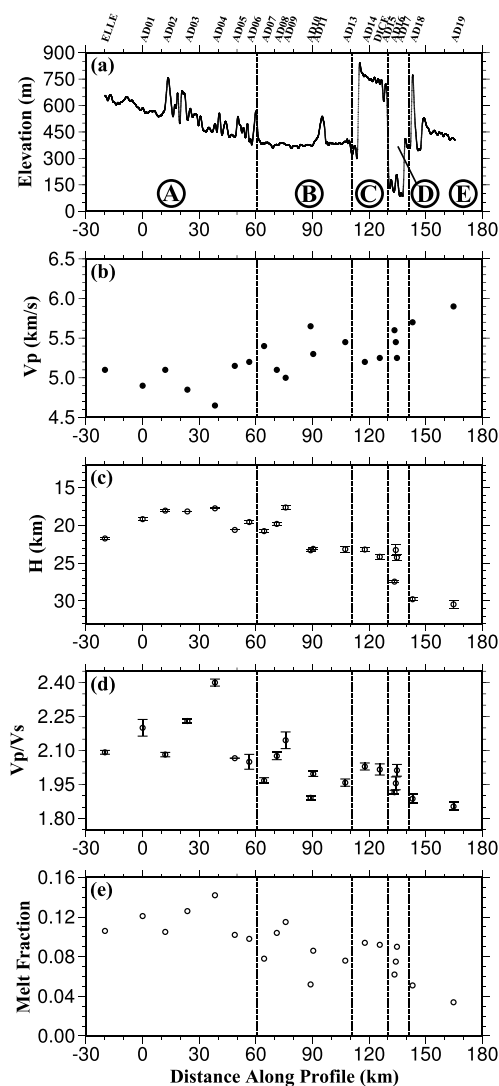


**Figure 7.** Cross-sectional profile views of the (a) elevation, (b)  $P$  wave velocity  $V_p$ , (c) crustal thickness  $H$ , (d)  $V_p/V_s$  velocity ratio  $\kappa$ , and (e) calculated melt fraction projected onto the bisected section line shown in Figure 1b.

The thinnest crust in the study area is characterized by a well-defined  $H$  of approximately  $17.6 \pm 0.2$  km beneath the center of the Tendaho graben at AD09, though Region A possesses the thinnest crust on average at  $19.3 \pm 1.5$  km (see Table 1). The thickest crust of  $30.4 \pm 0.5$  km is found beneath the northeastern end of the profile at station AD19. The Tendaho graben is characterized by an average  $H$  of  $21.3 \pm 2.3$  km, slightly thicker than that observed beneath Region A. The crustal thickness beneath Region C is  $22.6 \pm 0.8$  km, whereas that beneath the Dobi graben is  $24.3 \pm 1.9$  km.

Some of the values obtained previously are in good agreement with our findings. Hammond *et al.* [2011] reported a crustal thickness of  $29 \pm 2$  km at station LYDE, co-sited with AD19, which agrees with our observation of  $30.5 \pm 0.5$  km as well as with that of Makris and Ginzburg [1987]. They also obtained a thickness of  $24 \pm 3$  km at SRDE near station AD13, where we report a crustal thickness of approximately  $23.1 \pm 0.4$  km.

As we used  $V_p$  values which are consistently lower than the 6.0 km/s or greater employed by the previous studies, many of our resulting crustal thickness measurements are significantly smaller than those obtained heretofore. For instance, at station TEND which was co-sited with AD08, Dugda *et al.* [2005] and Hammond *et al.* [2011] both obtained an  $H$  value of 25 km with respective uncertainties of 1.5 km and 5 km, which

Only stations AD01, AD16, and DICE demonstrated higher-quality RF traces in the 0.08–0.8 Hz band, resulting in either a higher number of RFs used for the stacking or a higher confidence interval. Figure 5 depicts the  $H$ - $\kappa$  plot and corresponding RFs for station AD16 filtered at the 0.08–0.8 Hz band, possessing a  $P_{ss}$  arrival of negligible size but a significant offset of the  $P_{direct}$  phase of 0.60 s. This indicates that the sedimentary layer beneath AD16 in the Dobi graben has a high but indeterminate value of  $\kappa$ . The remaining 17 stations performed with higher quality at the higher frequency (0.2–1.2 Hz) band, as the higher corner frequencies revealed the existence of the  $P_{ss}$  phase as well as sharper ( $P_mS$ ) waveforms (Figure 6).

For the sake of clarity, we divide the study area into five distinguishable regions. Region A is the Red Sea rift flank beyond the southwestern border fault of the Tendaho graben and is composed of seven stations, Region B covers the Tendaho graben and the six stations located within, and Region C is sampled by the two stations in the relay zone between the Tendaho and Dobi grabens. Region D is the Dobi graben with three stations, and Region E is composed of the overlap zone to the northeast bounded by the Gulf of Aden and Dobi-Hanle rifts and is sampled by two stations. The results for each of the stations as well as the averaged results for the five regions are reported in Table 1. The station-specific results are also demonstrated in profile view in Figure 7.

### 3.2.1. Crustal Thickness Distribution

The crustal thickness observations have an asymmetric pattern (Figure 7c) defined by gradual thickening toward the southwest from the immediate southwestern rift flank and by relatively sharp thickening toward the northeast within Region E.

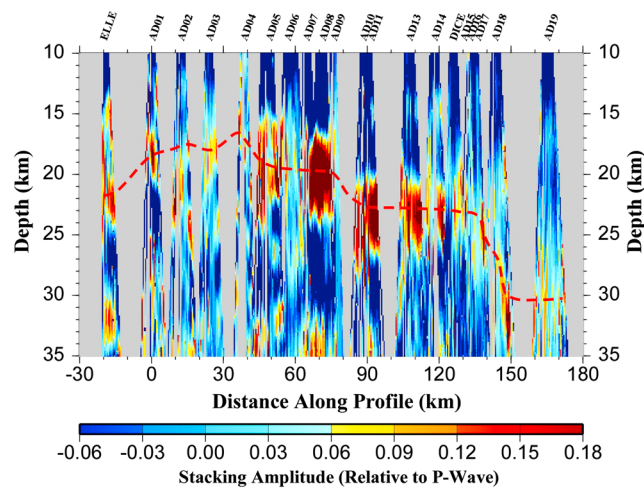


**Figure 8.** Profile of all 2277 normal moveout migrated RFs along the bisected section line (Figure 1b). The dashed red line indicates the peaks on the profile which correspond with the  $H$ - $\kappa$  results.

thickness, suggesting that areas with thinner crust have larger  $\kappa$  and lower  $V_p$  values. This is evidenced by the occurrence of the minimum regional  $\kappa$  value of  $1.870 \pm 0.024$  within Region E, where the crust is the thickest, and by the regionally maximum  $\kappa$  of  $2.160 \pm 0.126$  within Region A, which boasts the thinnest crust on average. These two areas possess  $V_p$  values of 5.80 and  $\sim 5.04$  km/s, respectively. The  $\kappa$  measurements systematically decrease toward the northeast from the southwestern end of the study area, and similar to our profile of crustal thickness, we note that values of  $\kappa$  diverge more rapidly toward the northeast than the southwest beyond the center of the Tendaho graben.

Our  $\kappa$  value of  $2.076 \pm 0.016$  for AD08 fits well with the reported values of  $2.16 \pm 0.05$  and  $2.02 \pm 0.15$  by Dugda et al. [2005] and Hammond et al. [2011], respectively. The latter study produced findings that are inconsistent with most of our observations inasmuch as they demonstrated a southwestward decrease in  $\kappa$ . For MILE, they reported  $1.88 \pm 0.11$  where we discovered a  $\kappa$  of  $2.230 \pm 0.011$ , and for LYDE they observed  $2.19 \pm 0.11$  where we constrained  $\kappa$  to  $1.853 \pm 0.018$ . These discrepancies could be the result of interference to the  $P_mS$  phase from surface or shallow heterogeneities at these stations, as discussed above for station AD19.

The Dobi graben does not correspond to any significant thinning of the crust relative to the Tendaho despite greater subsidence as indicated by a severe drop in elevation (Figure 7a). However, the average  $\kappa$  value amongst the three stations within the graben is comparable to that of the Tendaho graben, and the average  $V_p$  results for the two areas are statistically equivalent.

### 3.2.3. Migration of Receiver Functions

In order to demonstrate the quality of the RFs and the strength of the  $P_mS$  arrivals, we employ the station-specific  $\kappa$  and  $V_p$  values to migrate the RFs along the profile line (dashed line in Figure 1b). For a given station, we first compute an average  $V_s$  using the  $V_p$  and  $\kappa$  pair found for the station and apply it to calculate the coordinates of the ray piercing points from the surface to a depth of 35 km at an interval of 0.1 km. The piercing point location at a given depth is calculated by placing a hypothetical local event at the candidate depth and using the principle of equivalence between the ray parameters of the local  $S$  wave and the converting teleseismic  $P$  wave [Gao and Liu, 2013].

The topography of the Moho along the profile is evident as the line drawn through the high-stacking amplitude peaks (Figure 8). As expected, the depths of the amplitude peaks acquired in this fashion correlate well with the results of  $H$ - $\kappa$  stacking as reported in Table 1.

## 4. Discussion

### 4.1. Crustal Melting Distribution

Figure 7e shows the total melt fraction within the crust beneath each station calculated using the observed  $\kappa$  and the theoretical curve between  $\kappa$  and melt fraction (Figure 2b). As expected, the lateral distribution of melt fraction across the RSR, which ranges from about 14% to 3%, closely mirrors that of the  $\kappa$  observations.

is approximately 5 km thicker than our result of  $19.8 \pm 0.2$  km. Stations MILE and HARE, approximately colocated with stations AD03 and AD05, recorded thicknesses of  $33 \pm 5$  and  $25 \pm 1$  km, respectively, both of which are significantly higher than our measurements ( $18.2 \pm 0.1$  km in the case of the former,  $20.6 \pm 0.0$  km for the latter). Hammond et al. [2011] reported an  $H$  value of 31 km for DAME, though the quality of data was too poor, and the optimal value was taken from nearby stations. For station AD06, which is co-sited with DAME, we report an  $H$  value of  $19.5 \pm 0.2$  km.

### 3.2.2. $V_p/V_s$ Distribution

The resulting  $\kappa$  and  $V_p$  measurements (Figures 7d and 7b, respectively) demonstrate a spatial correlation with crustal

The average melt fraction for the five regions demonstrates an overall decreasing trend toward the north-east, with 11.4% melt for Region A, 8.5% for Region B, 10.2% for Region C, 8.4% for Region D, and 4.2% for Region E. The high melt fraction values beneath Regions A and B are slightly lower than the ~13% melt volume estimated using magnetotelluric measurements [Desissa *et al.*, 2013] associated with a 500 km<sup>3</sup> magma chamber underlying the Dabbahu magmatic segment. The higher melt volume observed beneath the Dabbahu magmatic segment, located approximately 100 km northwest of station AD08, is consistent with the fact that it is a more active section of the Manda-Hararo rift relative to the Tendaho graben [Rowland *et al.*, 2007; Field *et al.*, 2013]. These observations imply that partial melt within the crust is widespread throughout our study area, which is concurrent with the suggestion presented by Hammond *et al.* [2011] that melt pervades the crust throughout the Afar Depression, as well as the high  $V_p/V_s$  values from the RF study of Dugda *et al.* [2005]. The existence of significant melt within the crust is also consistent with the observed shallowing of earthquakes in the Afar relative to the MER [Daniels *et al.*, 2014]. Increased mantle temperatures beneath eastern Africa [Rooney *et al.*, 2012a] as well as thinned lithosphere and associated anomalous mantle temperature beneath the central Afar [Ferguson *et al.*, 2013] further support the indication of widespread melting processes beneath the East African rift in Ethiopia.

The melt fraction beneath the study area is significantly lower than that observed beneath mid-ocean ridges. For instance, Crawford *et al.* [1999] used compliance measurements within the East Pacific Rise to discern shallow pools of pure melt and lower crustal lenses with melt quantities as high as 18%. Their melt estimates agree with the findings of Sinton and Detrick [1992] who postulated that magma chambers in oceanic ridges are composed of fractionated crystalline “mush” with an upper bound of 50% melt overlain by lenses less than 3 km wide. Similarly, beneath the mid-Atlantic ridge, Canales *et al.* [2000] proposed a maximum partial melt percentage of  $17 \pm 3\%$  restricted to the lower crust, and MacGregor *et al.* [1998] utilized electromagnetic sounding to constrain a minimum of 20% melt in an axial magma chamber along the Reykjanes Ridge. Similarly, the seismic velocities beneath mid-ocean ridges [Crawford *et al.*, 1999; Hussenoeder *et al.*, 2002] are significantly lower than what we observed in Regions A and B. Beneath typical continental rift zones such as the Rio Grande and Baikal rifts, on the other hand, the average crustal velocities are significantly higher than those observed in Afar [West *et al.*, 2004; Mordvinova and Artemyev, 2010].

A model developed by Keir *et al.* [2009b] for magmatic injection during late-stage continental rifting proposed a middle to lower crust or uppermost mantle depth for melt supply directly beneath the Dabbahu rift segment. Anomalously low uppermost mantle velocities reported southwest of the RSR by Stork *et al.* [2013], as well as broad high-conductivity zones along the Moho revealed by magnetotelluric measurements beneath the Dabbahu magmatic segment [Desissa *et al.*, 2013], concur with the probability that magma beneath the RSR is sourced from a lower crustal or uppermost mantle reservoir. Hammond *et al.* [2011] expanded the results of their receiver function waveform modeling to infer lower crustal melt reservoirs permeating the entire Afar region.

#### 4.2. Spreading Center Migration

Earlier studies suggested that the RSR axis has migrated over time, concordant with a shift in both volumetric and spatial occurrence of volcanic activity as the result of variable spreading rates among the three rift arms [Tesfaye *et al.*, 2003; Hammond *et al.*, 2011]. Magmatism initiated at approximately 29 Ma with rhyolitic emplacements across a broad zone bounded by rift border faults. Subsequently, progressive eastward migration of strain from the border faults toward the Miocene rift axis proceeded until ~7 Ma [Wolfenden *et al.*, 2005], following which the RSR would have rotated into its current state. During the past 11 Ma, the MER propagated ~160 km N-NE in the Afar Depression with migration of the triple junction accommodated by extensive widespread magmatism within Afar [Tesfaye *et al.*, 2003; Wolfenden *et al.*, 2005].

The manner in which the RSR accompanied the movement of the triple junction is unclear. It has been suggested that the eastward migration of the RSR into its present-day configuration occurred as the result of a discrete rift jump from its paleolocation near the western Miocene border fault [Hammond *et al.*, 2011], which is similar to the behavior previously observed in mid-ocean ridges wherein ridge segments shift to exploit preexisting zones of weakness [Müller *et al.*, 2001]. The high melt fraction observed pervasively in Regions A and B, however, is more consistent with a model of gradual rather than “jumpy” migration of the RSR migration. This is consistent with the observation that both regions are underlain by anomalously low uppermost mantle velocities [Stork *et al.*, 2013]. According to this model, the high off-axial melt quantity

observed in Region A may be present as residual magmatic material remaining from a continuous eastward migration of the RSR axis.

### 4.3. Strain Localization and Upper-Lower Crustal Decoupling

Wolfenden *et al.* [2005] proposed the localization of strain within the southern RSR axis since  $\sim 15$  Ma, as did Manighetti *et al.* [1997] for the Gulf of Aden rift in the eastern Afar. Localization of extensional strain within the two rift arms has been postulated as the primary cause for the isolation of the continental blocks comprising the overlap zone [Tapponnier *et al.*, 1990] as well as lithosphere-scale thinning along the northern RSR boundary of the Danakil block [Bastow and Keir, 2011]. Rift-axial strain localization associated with magmatic provinces has been shown for both the MER [Ebinger and Casey, 2001] as well as the RSR and GOA propagators in the Afar [Manighetti *et al.*, 2001]. However, decreasing localization of strain in rift-axial uppermost crust and the resulting  $\sim 175$  km wide zone of measurable extension in the Afar [Kogan *et al.*, 2012] as well as an off-axis rift-orthogonal magmatic injection southeast of the northernmost MER [Keir *et al.*, 2011] indicate that the Afar is currently subjected to a broad strain field.

Casey *et al.* [2006] provided remote sensing and field analyses in the northern MER to restrict magmatic injections into the middle to upper crust along rift-axial magmatic provinces, thereby facilitating localized extensional strain within the  $\sim 10$  km seismogenic layer constrained by Keir *et al.* [2006b]. Strain within the Tendaho graben is expected to be similarly restricted to the uppermost crust prior to  $\sim 0.2$  Ma, at which time extrusive activity ceased, although minor localized extension within the TG axis still persists [Acocella *et al.*, 2008]. Our measurements of crustal thickness and inferred partial melt fractions, which are clearly not restricted to a rift-axial magmatic segment, suggest that deformation is more widespread in the lower crust concomitant with spatially voluminous melt reservoir emplacement. When combined with surface geological and geodetic observations, particularly with regard to the absence of localized uppermost crustal extension southwest of the RSR, our findings support the notion that in the lower crust, strain along our profile across the RSR is widely distributed, encompassed by a strain field stretching well into the southwestern Afar and the Dobi-Hanle rift system to the northeast while terminating with the rigid overlap zone.

The difference in deformation style and spatial distribution of extensional strain between the upper and lower crust suggests that the two crustal layers were decoupled during extension. Such decoupling has been suggested beneath both the Rio Grande rift [de Voogd *et al.*, 1988] and Basin and Range Province [MacCready *et al.*, 1997] in the western U.S. wherein the presence of a weak middle crust facilitates the decoupling of a ductile lower crust from a brittle upper crust. Models constructed for styles of rifting [Buck, 1991; Hopper and Buck, 1996] have emphasized the necessity of extremely weak rheologies in order to permit a lower crust to decouple from a strong upper crust, and Brace and Kohlstedt [1980] showed that a felsic crust will only deform in a brittle fashion to a depth of 10 km if the geothermal gradient is  $30^\circ\text{K/km}$ . Anomalous high surface heat flux as the result of a regionally elevated geotherm has been reported within central Afar [Lysak, 1992] and has been attributed either to enhanced magmatic activity associated with localized asthenospheric upwellings and decompressional melting [Hammond *et al.*, 2013] or to the proposed Afar plume [Oppenheimer and Francis, 1997; Cochran and Karner, 2007]. Surface eruptions hence only occur where localization of strain is sufficient to provide conduits for flow, which is constrained to axial rift segments. This particular mechanism for fault-controlled volcanism has been applied to the Hoggar swell in Algeria [Liu and Gao, 2010]. Sparse GPS measurements across the Tendaho graben do not currently possess the resolution required to preclude the observation of high strain rates in the southern RSR axis [Kogan *et al.*, 2012], and thus, we accede that additional constraints on the distribution of strain throughout the Afar are necessary to confirm our hypotheses.

## 5. Conclusions

Stacking of receiver functions recorded by the first broadband seismic array of such high resolution in the Afar Depression provides additional evidence supporting the notion that the lithosphere beneath the Red Sea rift in central Afar is currently in a state of transition between purely thinned continental crust and newly formed oceanic crust. The Red Sea rift axis is underlain by a crust with a highly reduced average  $V_p$  of 5.1 km/s as the result of an approximate 10% volume of partial melt. The measurements suggest that a regionally maximum degree of melt underlies the region to the southwest of the rift axis, possibly resulting from continuous eastward migration of the Red Sea rift axis since the late Miocene as well as focused melting due to asthenospheric upwelling to the west of the RSR. The widespread distribution of high melt

fraction values and regionally thinned crust indicate that extension beneath the Afar triple junction and southern RSR is occurring across a broad zone within the lower crust, which we believe to be deforming under ductile conditions through simultaneous magma injection, thereby decoupling it from the brittle upper crust.

#### Acknowledgments

Many people from Africa and the U.S. contributed to the planning, operation, and data analyses of the ALIE experiment. We thank the IRIS DMC for archiving our data and other data used in the study and the PASSCAL Instrument Center for providing the broadband seismometers and training. Special thanks are given to L. Carothers and N. Barstow of the PASSCAL Instrument Center for field and logistic support. Constructive suggestions from two anonymous reviewers significantly improved the manuscript. The field and data analysis work was supported by Statoil of Norway and the U.S. National Science Foundation under award EAR-1009946.

#### References

- Abbate, E., P. Passerini, and L. Zan (1995), Strike-slip faults in a rift area: A transect in the Afar Triangle, East Africa, *Tectonophysics*, *241*, 67–97.
- Acocella, V. (2010), Coupling volcanism and tectonics along divergent plate boundaries: Collapsed rifts from central Afar, Ethiopia, *Geol. Soc. Am. Bull.*, *122*, 1717–1728, doi:10.1130/B30105.1.
- Acocella, V., B. Abebe, T. Korme, and F. Barberi (2008), Structure of Tendaho Graben and Manda Hararo Rift: Implications for the evolution of the southern Red Sea propagator in central Afar, *Tectonics*, *27*, TC4016, doi:10.1029/2007TC002236.
- Acton, G. D., S. Stein, and J. F. Engeln (1991), Block rotation and continental extension in Afar: A comparison to oceanic microplate systems, *Tectonics*, *10*, 501–526.
- Acton, G. D., A. Tessema, M. Jackson, and R. Bilham (2000), The tectonic and geomagnetic significance of paleomagnetic observations from volcanic rocks from central Afar, Africa, *Earth Planet. Sci. Lett.*, *180*, 225–241.
- Ammon, C. J. (1991), The isolation of receiver effects from teleseismic *P* waveforms, *Bull. Seis. Soc. Am.*, *81*, 2504–2510.
- Ayalew, D., P. Barbey, B. Marty, L. Reisberg, G. Yirgu, and R. Pik (2002), Source, genesis, and timing of giant ignimbrite deposits associated with Ethiopian continental flood basalts, *Geochim. Cosmochim. Acta*, *66*, 1429–1448.
- Baker, J., L. Sneek, and M. Menzies (1996), A brief Oligocene period of flood volcanism in Yemen: Implications for the duration and rate of continental flood volcanism at the Afro-Arabian triple junction, *Earth Planet. Sci. Lett.*, *138*, 39–55.
- Barberi, F., and J. Varet (1977), Volcanism of Afar: Small-scale plate tectonics implications, *Geol. Soc. Am. Bull.*, *88*, 1251–1266.
- Bashir, L., S. S. Gao, K. H. Liu, and K. Mickus (2011), Crustal structure and evolution beneath the Colorado Plateau and the southern Basin and Range Province: Results from receiver function and gravity studies, *Geochem. Geophys. Geosyst.*, *12*, Q06008, doi:10.1029/2011GC003563.
- Bastow, I. D., and D. Keir (2011), The protracted development of the continent-ocean transition in Afar, *Nat. Geosci.*, *4*, 248–250, doi:10.1038/NGEO1095.
- Bastow, I. D., D. Keir, and E. Daly (2011), The Ethiopia Afar Geoscientific Lithospheric Experiment (EAGLE): Probing the transition from continental rifting to incipient seafloor spreading, *Spec. Pub. Geol. Soc. Am.*, *478*, 51–76, doi:10.1130/2011.2478(04).
- Beyene, A., and M. G. Abdelsalam (2005), Tectonics of the Afar Depression: A review and synthesis, *J. Afr. Earth Sci.*, *41*, 41–59, doi:10.1016/j.jafrearsci.2005.03.003.
- Bilham, R., R. Bendick, K. Larson, J. Braun, S. Tesfaye, P. Mohr, and L. Asfaw (1999), Secular and tidal strain across the Ethiopian rift, *Geophys. Res. Lett.*, *27*, 2789–2984.
- Bosworth, W., P. Huchon, and K. McClay (2005), The Red Sea and Gulf of Aden Basins: Phanerozoic evolution of Africa, *J. Afr. Earth Sci.*, *43*, 334–378, doi:10.1016/j.jafrearsci.2005.07.020.
- Brace, W. F., and D. L. Kohlstedt (1980), Limits on lithospheric stress imposed by laboratory experiments, *J. Geophys. Res.*, *85*, 6248–6252.
- Bridges, D. L., K. Mickus, S. S. Gao, M. G. Abdelsalam, and A. Alemu (2012), Magnetic stripes of a transitional continental rift in Afar, *Geology*, *40*, 203–206, doi:10.1130/G32697.1.
- Buck, W. R. (1991), Modes of continental extension, *J. Geophys. Res.*, *96*, 20,161–20,178, doi:10.1029/91JB01485.
- Caldwell, W. B., S. L. Klemperer, S. S. Rai, and J. F. Lawrence (2009), Partial melt in the upper-middle crust of the northwest Himalaya revealed by Rayleigh wave dispersion, *Tectonophysics*, *477*, 58–65, doi:10.1016/j.tecto.2009.01.013.
- Canales, J. P., J. A. Collins, J. Escartin, and R. S. Detrick (2000), Seismic structure across the rift valley of the Mid-Atlantic Ridge at 23° 20' (MARK area): Implications for crustal accretion processes at slow spreading ridges, *J. Geophys. Res.*, *105*, 28,411–28,425.
- Casey, M., C. Ebinger, D. Keir, R. Gloaguen, and F. Mohamed (2006), Strain accommodation in transitional rifts: Extension by magma intrusion and faulting in Ethiopian rift magmatic segments, in *The Afar Volcanic Province Within the East African Rift System*, vol. 259, edited by G. Yirgu, C. J. Ebinger, and P. K. H. Maguire, pp. 143–163, *Geo. Soc. London Spec. Pub.*, London, U. K., doi:10.1144/GSL.SP.2006.259.01.16.
- Chase, C. G. (1978), Plate kinematics: The Americas, East Africa, and the rest of the world, *Earth Planet. Sci. Lett.*, *37*, 355–368.
- Christensen, N. I. (1996), Poisson's ratio and crustal seismology, *J. Geophys. Res.*, *101*, 3139–3156.
- Clemens, J. D., and D. Vielzeuf (1987), Constraints on melting and magma production in the crust, *Earth Planet. Sci. Lett.*, *86*, 287–306.
- Cochran, J. R., and G. D. Karner (2007), Constraints on the deformation and rupturing of continental lithosphere of the Red Sea: The transition from rifting to drifting, in *Imaging, Mapping and Modelling Continental Lithosphere Extension and Breakup*, vol. 282, edited by G. D. Karner, G. Manatschal, and L. M. Pinheiro, pp. 265–289, *Geol. Soc. London Spec. Pub.*, London, doi:10.1144/SP282.13.
- Cornwell, D. G., G. D. Mackenzie, R. W. England, P. K. H. Maguire, L. M. Asfaw, and B. Oluma (2006), Northern Main Ethiopian Rift crustal structure from new high-precision gravity data, in *The Afar Volcanic Province Within the East African Rift System*, vol. 259, edited by G. Yirgu, C. J. Ebinger, and P. K. H. Maguire, pp. 307–321, *Geol. Soc. London Spec. Pub.*, London, doi:10.1144/GSL.SP.2006.259.01.23.
- Courillot, V., R. Armijo, and P. Tapponnier (1987), Kinematics of the Sinai triple junction and a two phase model of Arabia-Africa rifting, in *Continental Extensional Tectonics*, vol. 28, edited by M. P. Coward, J. F. Dewey, and P. L. Hancock, pp. 559–573, *Geol. Soc. London Spec. Pub.*, London, doi:10.1144/GSL.SP.1987.028.01.37.
- Crawford, W. C., S. C. Webb, and J. A. Hildebrand (1999), Constraints on melt in the lower crust and Moho at the East Pacific Rise, 9° 48' N, using seafloor compliance measurements, *J. Geophys. Res.*, *104*, 2923–2939.
- Daniels, K. A., I. D. Bastow, D. Keir, R. S. J. Sparks, and T. Menand (2014), Thermal models of dyke intrusion during development of continent-ocean transition, *Earth Planet. Sci. Lett.*, *385*, 145–153, doi:10.1016/j.epsl.2013.09.018.
- Desissa, M., N. E. Johnson, K. A. Whaler, S. Hautot, S. Fiseha, and G. J. K. Dawes (2013), A mantle magma reservoir beneath an incipient mid-ocean ridge in Afar, Ethiopia, *Nat. Geosci.*, *6*, 861–865, doi:10.1038/NGEO1925.
- de Voogd, B., L. Serpa, and L. Brown (1988), Crustal extension and magmatic processes: COCORP profiles from Death Valley and the Rio Grande rift, *Geol. Soc. Am. Bull.*, *100*, 1550–1567.
- Diehl, T., J. R. R. Ritter, and CALIXTO Group (2005), The crustal structure beneath SE Romania from teleseismic receiver functions, *Geophys. J. Int.*, *163*, 238–251, doi:10.1111/j.1365-246X.2005.02715.x.
- Dugda, M. T., A. A. Nyblade, J. Julia, C. A. Langston, C. J. Ammon, and S. Simiyu (2005), Crustal structure in Ethiopia and Kenya from receiver function analysis: Implications for rift development in eastern Africa, *J. Geophys. Res.*, *110*, B01303, doi:10.1029/2004JB003065.

- Dugda, M. T., A. A. Nyblade, and J. Julia (2007), Thin lithosphere beneath the Ethiopian Plateau revealed by a joint inversion of Rayleigh wave group velocities and receiver functions, *J. Geophys. Res.*, *112*, B08305, doi:10.1029/2006JB004918.
- Ebinger, C. J., and N. H. Sleep (1998), Cenozoic magmatism throughout East Africa resulting from impact of a single plume, *Nature*, *395*, 788–791.
- Ebinger, C. J., and M. Casey (2001), Continental breakup in magmatic provinces: An Ethiopian example, *Geology*, *29*, 527–530.
- Ebinger, C., A. Ayele, D. Keir, J. Rowland, G. Yirgu, T. Wright, M. Belachew, and I. Hamling (2010), Length and timescales of rift faulting and magma intrusion: The Afar rifting cycle from 2005 to present, *Ann. Rev. Earth Planet. Sci.*, *38*, 439–466, doi:10.1146/annurev-earth-040809-152333.
- Efron, B., and R. Tibshirani (1986), Bootstrap methods for standard errors, confidence intervals, and other measures of statistical accuracy, *Stat. Sci.*, *1*, 54–77.
- Ferguson, D. J., J. MacLennan, I. D. Bastow, D. M. Pyle, S. M. Jones, D. Keir, J. D. Blundy, T. Plank, and G. Yirgu (2013), Melting during late-stage rifting in Afar is hot and deep, *Nature*, *499*, 70–73, doi:10.1038/nature12292.
- Field, L., J. Blundy, A. Calvert, and G. Yirgu (2013), Magmatic history of Dabbahu, a composite volcano in the Afar Rift, Ethiopia, *Geol. Soc. Am. Bull.*, *125*, 128–147, doi:10.1130/B30560.1.
- Gao, S. S., and K. H. Liu (2013), Imaging mantle discontinuities using multiply-reflected P-to-S conversions, *Earth Planet. Sci. Lett.*, doi:10.1016/j.epsl.2013.08.025, in press.
- George, R., N. Rogers, and S. Kelley (1998), Earliest magmatism in Ethiopia: Evidence for two mantle plumes in one flood basalt province, *Geology*, *26*, 923–926.
- Hammond, W. C., and E. D. Humphreys (2000), Upper mantle seismic wave velocity: Effects of realistic partial melt geometries, *J. Geophys. Res.*, *105*, 10,975–10,986.
- Hammond, J. O. S., J. M. Kendall, G. W. Stuart, D. Keir, C. Ebinger, A. Ayele, and M. Belachew (2011), The nature of the crust beneath the Afar triple junction: Evidence from receiver functions, *Geochem. Geophys. Geosyst.*, *12*, Q12004, doi:10.1029/2011GC003738.
- Hammond, J. O. S., et al. (2013), Mantle upwelling and initiation of rift segmentation beneath the Afar Depression, *Geology*, *41*, 635–638, doi:10.1130/G33925.1.
- Hofmann, C., V. Courtillot, G. Feraud, P. Rochette, G. Yirgu, E. Ketefo, and R. Pik (1997), Timing of the Ethiopian flood basalt event and implications for plume birth and global change, *Nature*, *389*, 838–841.
- Hopper, J. R., and W. R. Buck (1996), The effect of lower crustal flow on continental extension and passive margin formation, *J. Geophys. Res.*, *101*, 20,175–20,194.
- Hussenoeder, S. A., G. M. Kent, and R. S. Detrick (2002), Upper crustal seismic structure of the slow spreading Mid-Atlantic Ridge, 35°N: Constraints on volcanic emplacement processes, *J. Geophys. Res.*, *107*, EPM 1–1 – 1–24, doi:10.1029/2001JB001691.
- Kähler, S., and R. Meissner (1983), Radiation and receiver pattern of shear and compressional waves as a function of Poisson's ratio, *Geophys. Prospecting*, *31*, 421–435.
- Kazmin, V. G., and A. F. Byakov (2000), Magmatism and crustal accretion in continental rifts, *J. Afr. Earth Sci.*, *30*, 555–568.
- Keir, D., G. W. Stuart, A. Jackson, and A. Ayele (2006a), Local earthquake magnitude scale and seismicity rate for the Ethiopian rift, *Bull. Seismol. Soc. Am.*, *96*, 2221–2230, doi:10.1785/0120060051.
- Keir, D., C. J. Ebinger, G. W. Stuart, E. Daly, and A. Ayele (2006b), Strain accommodation by magmatism and faulting as rifting proceeds to breakup: Seismicity of the northern Ethiopian rift, *J. Geophys. Res.*, *111*, B05314, doi:10.1029/2005JB003748.
- Keir, D., I. D. Bastow, K. A. Whaler, E. Daly, D. G. Cornwell, and S. Hautot (2009a), Lower crustal earthquakes near the Ethiopian rift induced by magmatic processes, *Geochem. Geophys. Geosyst.*, *10*, Q0AB02, doi:10.1029/2009GC002382.
- Keir, D., et al. (2009b), Evidence for focused magmatic accretion at segment centers from lateral dike injections captured beneath the Red Sea rift in Afar, *Geology*, *37*, 59–62, doi:10.1130/G25147A.1.
- Keir, D., C. Pagli, I. D. Bastow, and A. Ayele (2011), The magma-assisted removal of Arabia in Afar: Evidence from dike injection in the Ethiopian rift captured using InSAR and seismicity, *Tectonics*, *30*, TC2008, doi:10.1029/2010TC002785.
- Keranen, K., et al. (2004), Three-dimensional seismic imaging of a protoridge axis in the Main Ethiopian rift, *Geology*, *32*, 949–952, doi:10.1130/G20737.1.
- Kogan, L., S. Fisseha, R. Bendick, R. Reilinger, S. McClusky, R. King, and T. Solomon (2012), Lithospheric strength and strain localization in continental extension from observations of the East African Rift, *J. Geophys. Res.*, *117*, B03402, doi:10.1029/2011JB008516.
- Lahitte, P., P. Y. Gillot, and V. Courtillot (2003), Silicic central volcanoes as precursors to rift propagation: The Afar case, *Earth Planet. Sci. Lett.*, *207*, 103–116, doi:10.1016/S0012-821X(02)01130-5.
- Li, S., M. J. Unsworth, J. R. Booker, W. Wei, H. Tan, and A. G. Jones (2003), Partial melt or aqueous fluid in the mid-crust of Southern Tibet? Constraints from INDEPTH magnetotelluric data, *Geophys. J. Int.*, *153*, 289–304.
- Liu, K. H., and S. S. Gao (2010), Spatial variations of crustal characteristics beneath the Hoggar swell, Algeria, revealed by systematic analyses of receiver functions from a single seismic station, *Geochem. Geophys. Geosyst.*, *11*, Q08011, doi:10.1029/2010GC003091.
- Lysak, S. V. (1992), Heat flow variations in continental rifts, *Tectonophysics*, *208*, 309–323, doi:10.1016/0040-1951(92)90352-7.
- MacCready, T., A. W. Snoke, J. E. Wright, and K. A. Howard (1997), Mid-crustal flow during Tertiary extension in the Ruby Mountains core complex, Nevada, *Geol. Sci. Am. Bull.*, *109*, 1576–1594.
- MacGregor, L. M., S. Constable, and M. C. Sinha (1998), The RAMESSES experiment: III. Controlled-source electromagnetic sounding of the Reykjanes Ridge at 57°45'N, *Geophys. J. Int.*, *135*, 773–789.
- Mackenzie, G. D., H. Thybo, and P. K. H. Maguire (2005), Crustal velocity structure across the Main Ethiopian Rift: Results from two-dimensional wide-angle seismic modelling, *Geophys. J. Int.*, *162*, 994–1006, doi:10.1111/j.1365-246X.2005.02710.x.
- Makovsky, Y., and S. L. Klemperer (1999), Measuring the seismic properties of Tibetan bright spots: Evidence for free aqueous fluids in the Tibetan middle crust, *J. Geophys. Res.*, *104*, 10,795–10,825.
- Makris, J., and A. Ginzburg (1987), The Afar Depression: Transition between continental rifting and seafloor spreading, *Tectonophysics*, *141*, 199–214, doi:10.1016/0040-1951(87)90186-7.
- Mandal, P. (2006), Sedimentary and crustal structure beneath Kachchh and Saurashtra regions, Gujarat, India, *Phys. Earth Planet. Int.*, *155*, 286–299, doi:10.1016/j.pepi.2006.01.002.
- Manighetti, I., P. Tapponnier, V. Courtillot, S. Gruszow, and P.-Y. Gillot (1997), Propagation of rifting along the Arabia-Somalia plate boundary: The Gulfs of Aden and Tadjoura, *J. Geophys. Res.*, *102*, 2681–2710.
- Manighetti, I., P. Tapponnier, P. Y. Gillot, E. Jacques, V. Courtillot, R. Armijo, J. C. Ruegg, and G. King (1998), Propagation of rifting along the Arabia-Somalia plate boundary: Into Afar, *J. Geophys. Res.*, *103*, 4947–4974.
- Manighetti, I., P. Tapponnier, V. Courtillot, Y. Gallet, E. Jacques, and P.-Y. Gillot (2001), Strain transfer between disconnected, propagating rifts in Afar, *J. Geophys. Res.*, *106*, 13,613–13,665.

- McKenzie, D. P., D. Davies, and P. Molnar (1970), Plate tectonics of the Red Sea and East Africa, *Nature*, 226, 243–248, doi:10.1038/226243a0.
- Mohr, P. (1989), Nature of the crust under Afar: New igneous, not thinned continental, *Tectonophysics*, 167, 1–11, doi:10.1016/0040-1951(89)90290-4.
- Mordvinova, V. V., and A. A. Artemyev (2010), The three-dimensional shear velocity structure of lithosphere in the southern Baikal rift system and its surroundings, *Russ. Geol. Geophys.*, 51, 694–707, doi:10.1016/j.rgg.2010.05.010.
- Müller, R. D., C. Gaina, W. R. Roest, and D. L. Hansen (2001), A recipe for microcontinent formation, *Geology*, 29, 203–206.
- Nair, S. K., S. S. Gao, K. H. Liu, and P. G. Silver (2006), Southern African crustal evolution and composition: Constraints from receiver function studies, *J. Geophys. Res.*, 111, B02304, doi:10.1029/2005JB003802.
- Nakajima, J., T. Matsuzawa, A. Hasegawa, and D. Zhao (2001), Three-dimensional structure of  $V_p$ ,  $V_s$ , and  $V_p/V_s$  beneath northeastern Japan: Implications for arc magmatism and fluids, *J. Geophys. Res.*, 106, 21,843–21,857.
- Nyblade, A. A., and C. A. Langston (2002), Broadband seismic experiments probe the East African rift, *Eos Trans. AGU*, 83, 405–408, doi:10.1029/2002EO000296.
- Oppenheimer, C., and P. Francis (1997), Remote sensing of heat, lava and fumarole emissions from Erta 'Ale volcano, Ethiopia, *Int. J. Remote Sens.*, 18, 1661–1692.
- Pizzi, A., M. Coltorti, B. Abebe, L. Disperati, G. Sacchi, and R. Salvini (2006), The Wonji fault belt (Main Ethiopian Rift): Structural and geomorphological constraints and GPS monitoring, in *The Afar Volcanic Province Within the East African Rift System*, vol. 259, edited by G. Yirgu, C. J. Ebinger, and P. K. H. Maguire, pp. 191–207, Geol. Soc. London Spec. Pub., London, U. K., doi:10.1144/GSL.SP.2006.259.01.16.
- Press, W. H., S. A. Teukolsky, W. T. Vetterling, and B. P. Flannery (1992), *Numerical Recipes in FORTRAN 2nd ed.*, Cambridge Univ. Press, New York.
- Prodehl, C., K. Fuchs, and J. Mechie (1997), Seismic-refraction studies of the Afro-Arabian rift system—A brief review, *Tectonophysics*, 278, 1–13.
- Rooney, T., T. Furman, I. Bastow, D. Ayalew, and G. Yirgu (2007), Lithospheric modification during crustal extension in the Main Ethiopian Rift, *J. Geophys. Res.*, 112, B10201, doi:10.1029/2006JB004916.
- Rooney, T. O., C. Herzberg, and I. D. Bastow (2012a), Elevated mantle temperature beneath East Africa, *Geology*, 40, 27–30, doi:10.1130/G32382.1.
- Rooney, T. O., W. K. Hart, C. M. Hall, D. Ayalew, M. S. Ghiorso, P. Hidalgo, and G. Yirgu (2012b), Peralkaline magma evolution and the tephra record in the Ethiopian Rift, *Contrib. Mineral. Petrol.*, 164, 407–426, doi:10.1007/s00410-012-0744-6.
- Rowland, J. V., E. Baker, C. J. Ebinger, D. Keir, T. Kidane, J. Biggs, N. Hayward, and T. J. Wright (2007), Fault growth at a nascent slow-spreading ridge: 2005 Dabbahu rifting episode, Afar, *Geophys. J. Int.*, 171, 1226–1246, doi:10.1111/j.1365-246X.2007.03584.x.
- Ruegg, J. C. (1975), Main results about the crustal and upper mantle structure of the Djibouti region, in *Afar Depression of Ethiopia, Proceedings of an International Symposium on the Afar Region and Rift Related Problems*, vol. 1, edited by A. Pilger and A. Rosler, pp. 120–134, Schweizerbart, Stuttgart, Germany.
- Sheehan, A. F., G. A. Abers, C. H. Jones, and A. L. Lerner-Lam (1995), Crustal thickness variations across the Colorado Rocky Mountains from teleseismic receiver functions, *J. Geophys. Res.*, 100, 20,391–20,404.
- Sigmundsson, F. (1992), Tectonic implications of the 1989 Afar earthquake sequence, *Geophys. Res. Lett.*, 19, 877–880.
- Sinton, J. M., and R. S. Detrick (1992), Mid-ocean ridge magma chambers, *J. Geophys. Res.*, 97, 197–216.
- Stein, S., and R. G. Gordon (1984), Statistical tests of additional plate boundaries from plate motion inversions, *Earth Planet. Sci. Lett.*, 69, 401–412.
- Stork, A. L., G. W. Stuart, C. M. Henderson, D. Keir, and J. O. S. Hammond (2013), Uppermost mantle ( $P_n$ ) velocity model for the Afar region, Ethiopia: An insight into rifting processes, *Geophys. J. Int.*, 193, 321–328, doi:10.1093/gji/ggs106.
- Stuart, G. W., I. D. Bastow, and C. J. Ebinger (2006), Crustal structure of the Northern Main Ethiopian Rift from receiver function studies, in *The Afar Volcanic Province Within the East African Rift System*, vol. 259, edited by G. Yirgu, C. J. Ebinger, and P. K. H. Maguire, pp. 253–267, Geol. Soc. London Spec. Pub., London, doi:10.1144/GSL.SP.2006.259.01.20.
- Takei, Y. (2002), Effect of pore geometry on  $V_p/V_s$ : From equilibrium geometry to crack, *J. Geophys. Res.*, 107, ECV 6–1 – 6–12, doi:10.1029/2001JB000522.
- Taponnier, P., R. Armijo, I. Manighetti, and V. Courtillot (1990), Bookshelf faulting and horizontal block rotations between overlapping rifts in southern Afar, *Geophys. Res. Lett.*, 17, 1–4.
- Tesfaye, S., D. J. Harding, and T. M. Kusky (2003), Early continental breakup boundary and migration of the Afar triple junction, Ethiopia, *Bull. Geo. Soc. Am.*, 115, 1053–1067.
- Thurmond, A. K., M. G. Abdelsalam, and J. B. Thurmond (2006), Optical-radar-DEM remote sensing data integration for geological mapping in the Afar Depression, Ethiopia, *J. Afr. Earth Sci.*, 44, 119–134.
- Varet, J. (1978), *Geology of Central and Southern Afar (Ethiopia and Djibouti Republic)*, pp. 1–124, CNRS, Paris, France.
- Wang, T. K., and C. H. Pan (2001), Crustal Poisson's ratio of Eastern Taiwan from OBS data modeling, *Terr., Atmos. Ocean. Sci.*, 12, 249–268.
- Watanabe, T. (1993), Effects of water and melt on seismic velocities and their application to characterization of seismic reflectors, *Geophys. Res. Lett.*, 20, 2933–2936.
- West, M., J. Ni, W. S. Baldrige, D. Wilson, R. Aster, W. Gao, and S. Grand (2004), Crust and upper mantle shear wave structure of the southwest United States: Implications for rifting and support for high elevation, *J. Geophys. Res.*, 109, B03309, doi:10.1029/2003JB002575.
- Whaler, K. A., and S. Hautot (2006), The electrical resistivity structure of the crust beneath the northern Main Ethiopian Rift, in *The Afar Volcanic Province Within the East African Rift System*, vol. 259, edited by G. Yirgu, C. J. Ebinger, and P. K. H. Maguire, pp. 293–305, Geol. Soc. London Spec. Pub., London, U. K., doi:10.1144/GSL.SP.2006.259.01.22.
- Wolfenden, E., C. Ebinger, G. Yirgu, A. Deino, and D. Ayalew (2004), Evolution of the northern Main Ethiopian rift: Birth of a triple junction, *Earth Planet. Sci. Lett.*, 224, 213–228, doi:10.1016/j.epsl.2004.04.022.
- Wolfenden, E., C. Ebinger, G. Yirgu, P. R. Renne, and S. P. Kelley (2005), Evolution of a volcanic rifted margin: Southern Red Sea, Ethiopia, *Bull. Geo. Soc. Am.*, 117, 846–864, doi:10.1130/B25516.1.
- Yeck, W. L., A. F. Sheehan, and V. Schulte-Pelkum (2013), Sequential H- $\kappa$  stacking to obtain accurate crustal thicknesses beneath sedimentary basins, *Bull. Seis. Soc. Am.*, 103, 2142–2150, doi:10.1785/0120120290.
- Yuan, X., S. V. Sobolev, and R. Kind (2002), Moho topography in the central Andes and its geodynamic implications, *Earth Planet. Sci. Lett.*, 199, 389–402.
- Zelt, B. C., and R. M. Ellis (1999), Receiver-function studies in the Trans-Hudson Orogen, Saskatchewan, *Can. J. Earth Sci.*, 36, 585–603.
- Zhu, L. P., and H. Kanamori (2000), Moho depth variation in southern California from teleseismic receiver functions, *J. Geophys. Res.*, 105, 2969–2980.